J. Meas. Sci. Instrum., 2025, 16(4): 473-485. http://jmsi.publish.founderss.cn/
DOI: 10.62756/jmsi.1674-8042.2025046 jmsi@nuc.edu.cn

Human presence detection and heart rate estimation algorithm based on millimeter-wave radar

ZHU Xinxing[1], GAO Yixuan[1], LI Mingchao[1], WU Enkang[1], GU Xiaofeng[1], LIANG Junge[1,2*], YU Tian[1*], WANG Cong[3]

1. School of Integrated Circuits, Jiangnan University, Wuxi 214122, China;
2. RFIC Center, Kwangwoon University, Seoul 01897, Republic of Korea;
3. School of Electronics and Information Engineering, Harbin Institute of Technology, Harbin 150001, China

***Corresponding author:** LIANG Junge (liangjunge@hotmail.com); YU Tian (yutian@jiangnan.edu.cn)

Received: May 30, 2025 **Revised:** July 2, 2025 **Accepted:** July 28, 2025

Abstract: Millimeter-wave radar, with advantages such as non-contact penetration detection and privacy protection, has become a promising solution for unobtrusive monitoring in the field of smart elderly care. To solve the problem of whether there are human body in the elderly care scene, this study proposed a method for judging the presence of a human body based on adaptive dual thresholds to reduce invalid vital sign detection in an empty environment. This method used a low-frequency energy ratio as the core judgment basis. It combined adaptive thresholds to accurately judge the presence of human targets, effectively reducing false detections caused by background interference. In addition, given the defect that variational mode extraction (VME) needs to rely on manual parameter adjustment based on empirical values, the crown porcupine optimization (CPO) algorithm is introduced to optimize the VME parameters adaptively, and the optimized VME is used to reconstruct the heartbeat signal to improve the signal purity. Then, the multiple signal classification (MUSIC) algorithm was used for spectrum analysis to improve the accuracy of heart rate estimation. The results show that in the experimental judgment of personnel, the miss rate in the case of personnel presence is 2.2%, and the false alarm rate in the case of no personnel is only 3.2%; the root mean square error and mean absolute error of the proposed heart rate (HR) estimation method are reduced by 4.4 beat per minute and 3.05 beat per minute respectively compared with the traditional VME, verifying its excellence.

Key words: human presence detection; FMCW radar; adaptive dual threshold; improved VME; multiple signal classification

0 Introduction

As the global aging trend intensifies, the health of the elderly has become a core issue of social concern[1]. Studies have shown that timely intervention measures for the elderly can significantly reduce the incidence of fatal diseases among the elderly[2]. Therefore, the demand for smart elderly care technology is increasing, especially for the elderly living alone at home. In recent years, with the development of non-contact sensing technology, non-contact devices are attracting increasing attention, which do not need to be worn, have higher comfort, and are more suitable for forgetful elderly people[3].

Contactless sensing technologies include visible light sensing, acoustic sensing, and various radio frequency technology solutions. Radio frequency solutions can be divided into solutions based on Wi-Fi signals[4], radio frequency identification (RFID)[5], and radar sensing solutions. Radar has become an important research direction in non-contact vital signs detection due to its good penetration, high sensitivity, and strong privacy protection[6]. RF solutions mainly use radar as detection equipment, which can be divided into continuous wave (CW) Doppler radar[7], ultra-wideband (UWB) radar[8], and frequency modulated continuous wave (FMCW) radar[9]. FMCW millimeter wave radar has both the high sensitivity of CW radar and the ranging performance of UWB radar, and has become the mainstream solution.

Vital sign detection is of great significance to ensure the safety of the elderly. With the increase in age, the probability of elderly people suffering from chronic diseases increases significantly. The early stage of the pathological process is often asymptomatic. By detecting heart rate, a variety of chronic diseases in the elderly can be effectively prevented[10]. In a home-based elderly care environment, millimeter-wave radar is used directly to detect the vital signs of humans. When no human body is present, the millimeter-wave radar will be affected by the indoor background signals[11]. Since these signals may contain low-frequency fluctuation signals similar to vital signs, if these

signals are processed directly, it is very easy to cause false vital sign detection results[12]. In the elderly care scenario, it will mislead the judgment of nursing staff and bring serious consequences. Therefore, it is important to make an accurate human body presence judgment before vital sign detection. Deiana et al.[13] proposed a method of using 24 GHz frequency modulated continuous wave radar to detect the presence in office environments by detecting small movements of people, such as typing. However, this method is highly dependent on the motion signals of the target being detected. When the human body remains still, especially in the elderly who like to sit still, the accuracy will be greatly reduced. Regev et al.[14] proposed to detect the presence of a human body through tiny breathing movements and estimate the breathing rate. They used sleeping babies and people sitting still as targets, and did not verify the situation where no one was present or the situation where there was someone switching between them.

In addition, since the chest displacement amplitude generated by the heartbeat signal is weak, it is easily affected by respiratory harmonics, environmental noise, and random body movements, making it difficult to effectively extract its frequency characteristics[15]. To address these problems, Qu et al.[16] proposed an improved adaptive parametric variational mode decomposition (IAPVMD) method to adaptively select the optimal number of modes and the optimal penalty coefficient to reconstruct the heartbeat signal. This method mainly focuses on the separation of frequency and energy dimensions, and there is room for improvement in the extraction of weak phase changes. Duan[17] proposed using VME to extract heartbeat phase information and using chirp Z transform (CZT) to analyze the frequency components of the heartbeat. However, CZT is prone to spectrum leakage under low signal-to-noise ratio conditions, which makes it difficult to distinguish between the heartbeat fundamental frequency and respiratory harmonic components.

Therefore, this paper addresses the remaining problems of the above algorithms and makes the following efforts. 1) By calculating the low-frequency energy ratio and combining the adaptive dual-threshold strategy, the threshold can be dynamically adjusted according to the change of environmental noise, and a logical judgment can be made on the human presence status to accurately distinguish whether a person is present or not. By introducing the dual-threshold mechanism, false positives and false negatives can be effectively reduced, the process of identifying state transitions can be stabilized, and the accuracy and robustness of the judgment results can be guaranteed. 2) CPO is used to optimize the initial center frequency and penalty factor of VME, and the optimized VME is used to reconstruct the heartbeat signal. Then MUSIC is used for frequency analysis to improve the accuracy and stability of HR estimation.

1 Theory and method overview

1.1 FMCW radar fundamentals

The FMCW millimeter-wave radar consists of an FMCW signal synthesizer, a power amplifier, a transmitting antenna, a receiving antenna, a low-noise amplifier, a mixer, and an analog-to-digital converter. The contactless FMCW radar system is shown in Fig.1.

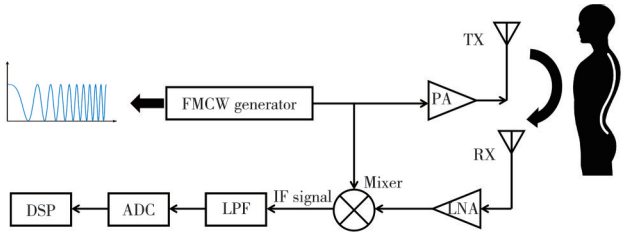

Fig. 1 Block diagram of radar system

The FMCW signal synthesizer generates a linear frequency modulated wave signal and periodically emits multiple linear frequency modulated pulses. Each pulse is called a chirp and can be expressed as

$$S_{\mathrm{T}}(\mathrm{t})=A_{\mathrm{T}}\cos\left[2\pi f_0 t+\pi\frac{B}{T_{\mathrm{c}}}t^2+\varphi(t)\right], \tag{1}$$

where A_{T} is the amplitude of the transmitted signal, f_0 is the starting frequency of the chirp signal, B is the bandwidth of the chirp signal, T_{c} is its modulation period, B/T_{c} is expressed as the linear frequency modulation slope, and $\varphi(t)$ is the phase noise.

The signal transmitted by the transmitting antenna is reflected by the target and received by the receiving antenna, which will cause a transmission time delay, which can be expressed as

$$\tau=\frac{2r(t)}{c}, \tag{2}$$

where c is the speed of light and $r(t)$ is expressed as

$$r(\mathrm{t})=r_0+\Delta r(t), \tag{3}$$

where r_0 is the radial distance between the human body and the radar, and $\Delta r(t)$ is the vibration displacement of the chest caused by human breathing and heartbeat. The reflected echo signal can be expressed as

$$S_{\mathrm{R}}(t)=A_{\mathrm{R}}\cos\left[2\pi f_0(t-\tau)+\pi\frac{B}{T_{\mathrm{c}}}(t-\tau)^2+\varphi(t-\tau)\right], \tag{4}$$

where A_{R} is the amplitude of the echo signal. The

transmit signal and the receive signal of the FMCW radar are mixed through a mixer, and a low-pass filter is used to generate an intermediate frequency signal (IF).

$$S_{\mathrm{IF}}(t)=A_{\mathrm{T}}A_{\mathrm{R}}\exp\left[\mathrm{j}\left(2\pi f_{\mathrm{IF}}\mathrm{t}+2\pi f_0\tau+\pi\frac{B}{T_{\mathrm{c}}}\tau^2+\Delta\varphi(t)\right)\right], \tag{5}$$

where $f_{\mathrm{IF}}=\dfrac{B\tau}{T_{\mathrm{c}}}$ is the intermediate frequency signal frequency, $\Delta\varphi(t)=\varphi(t)-\varphi(t-\tau)$ is the phase noise difference caused by the transmission time delay. Since the actual distance $r(t)$ from the radar to the human body is relatively small, $\pi\left(\dfrac{B}{T_{\mathrm{c}}}\right)\tau^2$ and $\Delta\varphi(t)$ can be ignored, and the intermediate frequency signal can be simplified to

$$S_{\mathrm{IF}}(\mathrm{t})=A_{\mathrm{T}}A_{\mathrm{R}}\exp\left[j\left(4\pi\frac{Br(t)}{cT_{\mathrm{c}}}\mathrm{t}+4\pi\frac{f_0r(t)}{c}\right)\right]. \tag{6}$$

So the phase shift is

$$\varphi_{\mathrm{IF}}=\frac{4\pi}{\lambda}\Delta r(t), \tag{7}$$

where λ is the wavelength of the millimeter-wave radar.

1.2 Vital sign signal analysis

Fig.2 shows the transmitted and received signals of an FMCW radar.

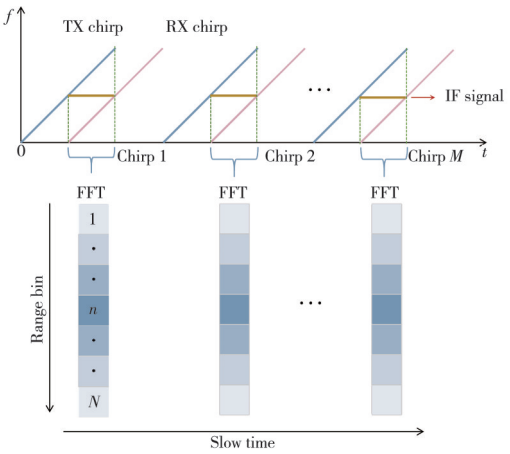

Fig. 2 Fundamental principle of FMCW radar

After mixing, the IF signal is obtained. Within a single chirp, the received echo signal is sampled, forming the fast time dimension. A Fourier transform, specifically a one-dimensional fast Fourier transform (1D-FFT), is then performed to extract the distance r_0 between the radar and a static target. After distance estimation, the signal at the same range bin is typically observed across multiple chirp periods, forming the slow time dimension. At the target range bin, further analysis of the phase variations over the slow time dimension enables the extraction of fine displacement information, allowing the detection of micro-movements of the target. At that distance gate, the phase can be further analyzed to obtain information on the small displacement of the target.

During the breathing process, the human body's lungs contract and relax periodically, which causes the chest cavity to fluctuate in the front-to-back direction, with an amplitude of 1 mm to 12 mm. The heartbeat movement originates from the contraction and relaxation of the heart. Although the amplitude is smaller, it also causes a tiny periodic displacement of the chest cavity, usually between 200 μm to 500 μm. Both human breathing and heartbeat are low-frequency movements, with the human breathing frequency ranging from 0.1 Hz to 0.5 Hz and the heartbeat frequency ranging from 0.8 Hz to 2 Hz. Since the frequency ranges of the two are different, they can be distinguished in the frequency domain.

Under ideal conditions, the phase at time t can be expressed as

$$\Delta\theta=\frac{4\pi(r_{\mathrm{b}}(t)+r_{\mathrm{h}}(t))}{\lambda}. \tag{8}$$

Among them, $r_{\mathrm{b}}(t)$ represents the displacement information related to the chest movement caused by breathing, and $r_{\mathrm{h}}(t)$ represents the displacement information related to the chest movement caused by heartbeat. Therefore, the vital sign signal can be represented by

$$\Delta r(t)=r_{\mathrm{b}}(t)+r_{\mathrm{h}}(t)=\mathrm{A_b}\sin\left(2\pi f_{\mathrm{b}}t\right)+\mathrm{A_h}\sin\left(2\pi f_{\mathrm{h}}t\right), \tag{9}$$

where A_{b} and A_{h} are the amplitudes of breathing and heartbeat, respectively; f_{b} and f_{h} are the frequencies corresponding to breathing and heartbeat, respectively. Therefore, the heartbeat mode can be extracted from the vital sign signal, and the heart rate can be estimated.

1.3 Method overview

The signal processing flow of this paper is shown in Fig.3, which consists of two parts. 1) Human presence judgment. After preprocessing the radar data, the phase data is analyzed in the frequency domain to obtain the spectral characteristics of the time series signal. Subsequently, the low-frequency energy ratio in the entire time window is calculated as an important indicator for measuring the weak life activities of the target. Based on the low-frequency energy ratio, a dynamic threshold is set and used as the logical basis for subsequent human presence judgment to achieve non-contact human presence perception. 2) HR estimation. Process the phase information at the range gate where the human target is located, use the CPO algorithm to optimize the penalty

factor and initial center frequency of VME, and automatically obtain the most suitable parameter combination. Use the improved VME to reconstruct the phase signal to extract a more accurate heartbeat signal, and then use MUSIC to perform frequency domain analysis on the reconstructed signal to accurately estimate the HR.

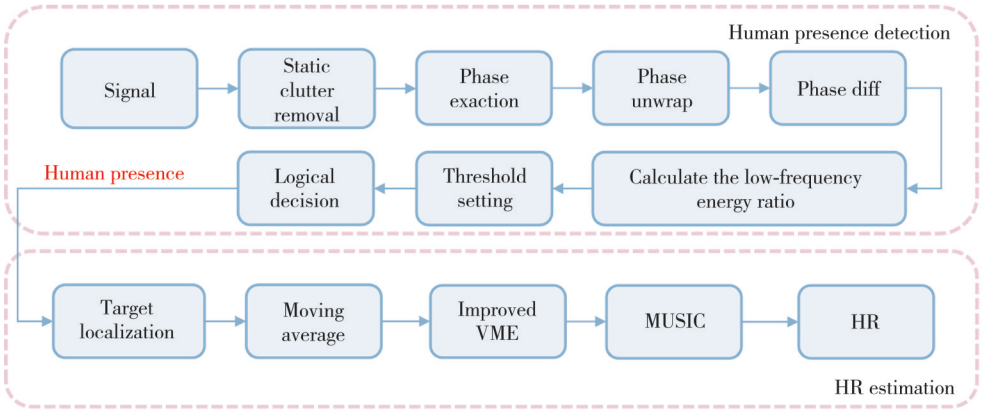

Fig. 3 Flow diagram of signal processing

2 Proposed method

2.1 Human presence detection and preprocessing

Before detecting vital signs, it is necessary to first determine whether there is a human target in the detection area to avoid unnecessary detection of the air environment. The IF signal obtained from the millimeter-wave radar is processed with an FFT along the fast-time dimension to extract range information. A matrix is then constructed using the range profiles and the time windows. The matrix is denoted as $x[m, l]$ (m is the distance unit index, l is the number of frames, $l \in [1, L]$, L is the time window length).

By using the phase change of the intermediate frequency and signal caused by the displacement of the human chest wall, breathing and heartbeat information can be obtained. After the original radar data is Fourier transformed, static clutter will be generated due to the existence of the radar's DC component and the reflection of static objects such as walls, affecting the distance positioning of human targets. Within a certain time window, averaging the signal energy can reflect the interference component of static clutter. Subtracting the mean from the original signal can effectively suppress static clutter, which can be expressed as

$$x[m,l] = x[m,l] - \frac{1}{L}\sum_{l=1}^{L} x[m,l]. \tag{10}$$

As shown in Fig.4, it is a distance-time diagram before and after removing static clutter. In Fig 4 (a), the human target is located at 0.5 m from the radar, 0 m is the radar DC component, and 1 m and 2 m are static clutter caused by static objects such as tables and chairs. In Fig.4 (b), after using the algorithm, the static clutter in the environment is successfully removed, making the echo signal of the human target clearer and more prominent.

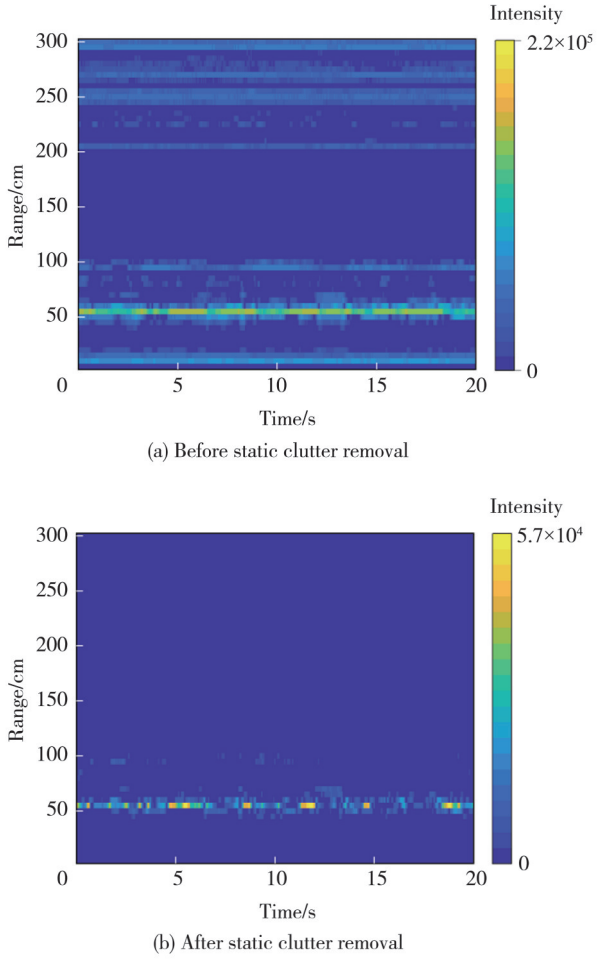

Fig. 4 Range-time plot

Due to the micro-motion of the human body, the energy fluctuations in the distance spectrum will be obvious. Therefore, the energy characteristics of the distance where the human target is located can be effectively enhanced by accumulating the distance

dimension FFT results of the same range gate within a certain time window, which can be expressed as

$$x[m]=\sum_{l=1}^{L}\left|x'[m,l]\right|. \tag{11}$$

As shown in Fig.5, the distance d of the human target can be determined by the maximum value of the signal amplitude. Take the corresponding phase information for each range gate, and use the arctan function to extract the phase at the target. Since the value range of the arctan function is $[-\pi,\pi]$, when the phase crosses $-\pi$ and π, the phase will jump, resulting in discontinuous phase signals, so the phase signal needs to be unwrapped to obtain the true value of the phase. So

$$\phi_m(l)=\begin{cases}\phi_m(l)-2\pi, \phi_m(l)-\phi_m(1-1)>\pi,\\ \phi_m(l)+2\pi, \phi_m(l)-\phi_m(l-1)<\pi.\end{cases} \tag{12}$$

Then, in order to enhance the low-frequency components in the phase, the changes in the small movements in the phase sequence are extracted, and the phase is first-order differentiated to highlight the phase disturbance caused by human breathing and heartbeat.

$$\phi_m'(l)=\phi_m(l)-\phi_m(l-1). \tag{13}$$

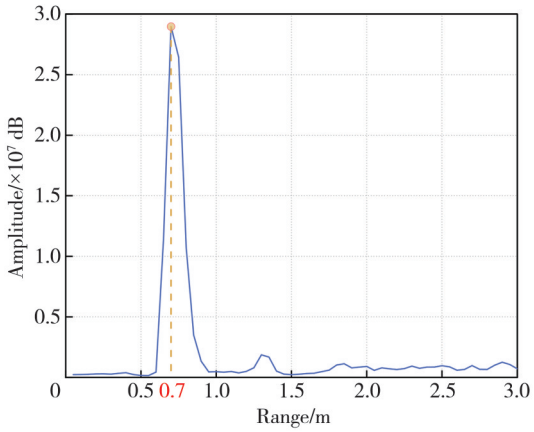

Fig. 5 Position of human after signal accumulation

Perform a one-dimensional Fourier transform on the phase data in the time dimension to obtain $A(f,m)$, where f is the frequency, which facilitates the analysis of the spectral characteristics of each range gate in time. The spectral energy of each range gate is accumulated in the frequency dimension, and the total energy at the mth range gate is defined as

$$E_{total}(m)=\sum_{f=1}^{F}A(f,m). \tag{14}$$

Since the physiological signals of the human body are mainly manifested as periodic signals in the low-frequency band, the energy in the low-frequency band f_1 to f_2 is extracted as an important basis for judging the presence of the human body. In this paper, f_1 and f_2 are taken as 0.2 Hz and 0.5 Hz, respectively.

$$E_{low}(m)=\sum_{f=f_1}^{f_2}A(f,m). \tag{15}$$

Fig.6 is a spectrum energy diagram of the presence or absence of human bodies.

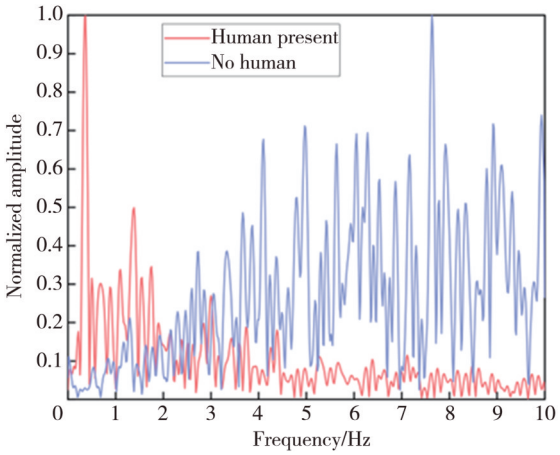

Fig. 6 Spectrogram with and without human presence

It can be clearly seen that when there is a human body in the environment, the energy proportion at the low frequency is higher than when there is no human body. For each range gate, calculate the proportion of the energy of the breathing frequency band in the total energy. If the low-frequency energy proportion of a range gate is high, it may mean that there is a human body. The low-frequency energy proportion can be expressed as

$$r_l(m)=\frac{E_{low}(m)}{E_{total}(m)}. \tag{16}$$

Adaptive thresholds $T_1(l)$ and $T_2(l)$ are set. If $T_1(l)$ is too large, it is easy to cause missed detection. A human with weak vital signs may not be detected. If it is too small, the detection will become loose, and slight energy will be judged as a human, resulting in false detection. Similarly, if $T_2(l)$ is too large or too small, it may lead to false positives or false negatives. Therefore, to maintain a balance between detection stability and sensitivity, $T_1(l)$ is 70% of the low-frequency energy proportion of all range gates in the current frame, which is used to determine the transition from no one to someone; $T_2(l)$ is 30% of the low-frequency energy proportion of all range gates in the current frame, which is used to determine the transition from someone to no one. Compared with the traditional fixed threshold, the adaptive threshold can be adaptively adjusted according to the energy characteristics of the current frame, and the dual threshold strategy is introduced to significantly improve the response sensitivity and judgment stability of the appearance and disappearance of human targets in dynamic environments.

The result judgment flow chart is shown in Fig. 7. When there is no historical judgment result, the initial judgment is made based on the low-frequency energy ratio of the target distance gate in the current frame.

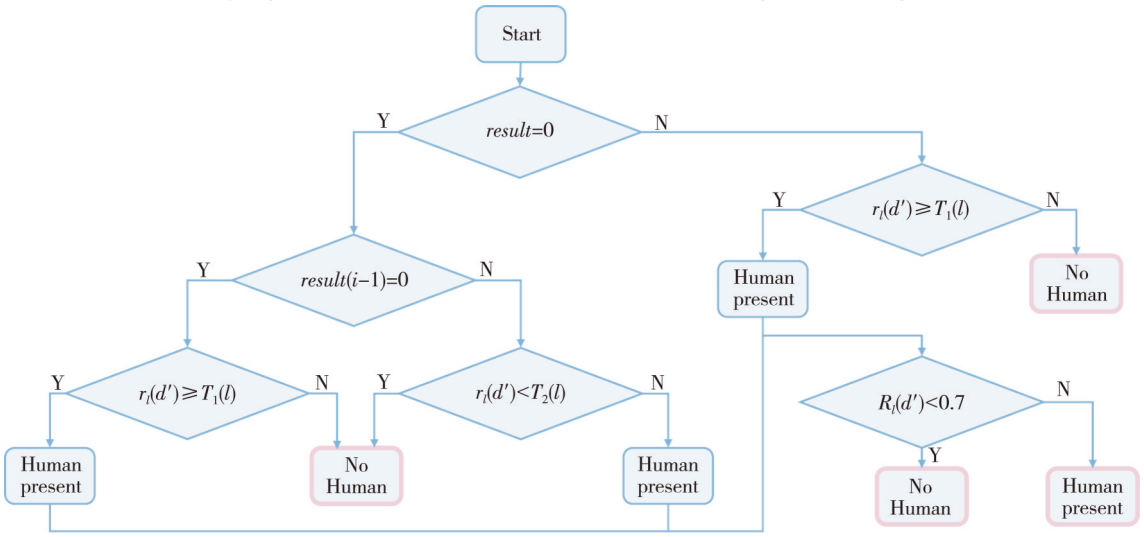

Fig. 7 Flow diagram of human presence detection

If the low-frequency energy ratio at the target distance gate is greater than $T_1(l)$, then the preliminary judgment is that the human body exists. Otherwise, it is judged that there is no human body. If there is a historical detection result, and the previous frame judged that there was no human body, the low-frequency energy ratio at the target distance gate is greater than $T_1(l)$, then the preliminary judgment is that the human body exists. Otherwise, there is no human body. If there are historical detection results, and the last time it was judged that there was a human target, the low-frequency energy ratio at the target distance gate is less than $T_2(l)$, then the human target is considered to have disappeared, otherwise the judgment of the human presence is maintained.

Fig.8 (a) is a comparison of the low-frequency energy ratio and threshold from no one to someone. In the first 25 s, the low-frequency energy ratio is mostly lower than the low threshold, indicating an unmanned state. When the energy ratio is between the low threshold and the high threshold, it is a transitional stage, and the state is changed only after the conditions are met several times in a row, so it is still an unmanned state. At 25 s, it jumps from below the low threshold to above the high threshold, and it is judged that someone has appeared. Fig. 8(b) is a comparison of the low-frequency energy ratio and threshold from someone to no one. At 30 s, the low-frequency energy ratio drops from above the high threshold to below the low threshold, and it can be judged that the person has left and entered the "unmanned state".

When the detection result preliminarily determines that there is a human target, it is necessary to further verify the body's existence status to determine whether the detected target is credible. Calculate the ratio of the energy near the current frame target d' to the total energy near the maximum echo energy in the entire time window by

$$Rate_l(m)=\frac{\sum_{d'-1}^{d'+1}x[i]}{\sum_{d-1}^{d+1}x[i]}. \tag{17}$$

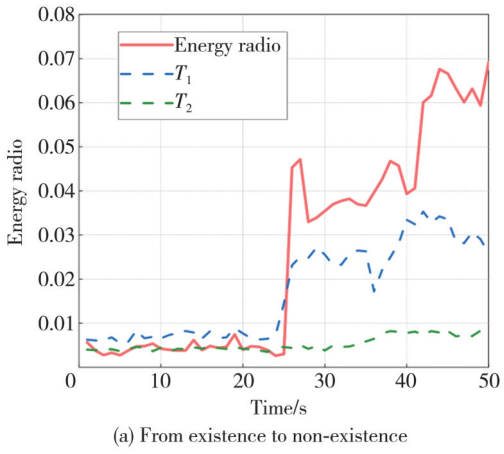

(a) From existence to non-existence

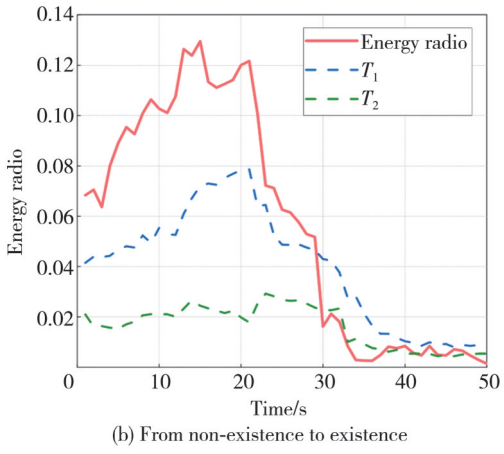

(b) From non-existence to existence

Fig. 8 Low-frequency energy ratio compared against threshold

When the energy ratio is less than 0.7, it is considered that there is no human body. The energy ratio $Rate_l$ can eliminate false detections caused by non-living targets or environmental noise, thereby improving the accuracy of detection.

When the presence of a human target is determined, the phase at the human target is extracted, unwrapped, and differentiated. Although phase differentiation can enhance the characteristics of small movements, it is easy to amplify the high-frequency noise in the signal, thereby introducing non-physiological fluctuations and interfering with subsequent vital sign estimation. Therefore, a sliding average method is used to smooth the signal and effectively suppress high-frequency noise.

$$y(l)=\frac{1}{N}\sum_{k=m-\frac{l_w}{2}}^{m+\frac{l_w}{2}}\phi'(k), \tag{18}$$

where l_w is the length of the sliding window.

Fig.9 shows the phase extraction, unwrapped, difference and sliding average at the target.

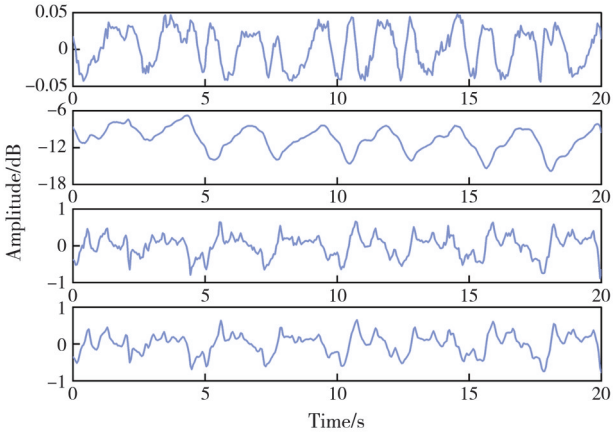

Fig. 9 Raw phase, unwrapped phase, differential phase and phase after moving average filtering

2.2 Improved VME algorithm

The VME[18] algorithm can accurately extract the characteristic components in the target frequency band based on the prior frequency information of the signal without presetting the number of modes, thereby effectively separating the signal of interest. VME constrains the modes so that the spectrum energy is tightly concentrated near their respective center frequencies, thereby minimizing their bandwidth as much as possible while retaining the desired modal information and avoiding interference from irrelevant components.

The VME algorithm assumes that the input signal $f(t)$ can be represented as the sum of the desired pattern $u_d(t)$ and the residual term $r(t)$.

$$f(t)=u_d(t)+r(t). \tag{19}$$

The desired signal is near a specific center frequency ω_d, so it can be minimized by

$$J_1=\left\| \partial t\left[\left(\delta(t)+\frac{\mathrm{j}}{\pi t}\right)u_d(t)\right]\mathrm{e}^{-\mathrm{j}\omega_d t}\right\|_2^2, \tag{20}$$

where $\delta(\cdot)$ is a Dirac distribution. In order to fully extract the target signal component, the spectrum overlap between the residual term and the desired mode should be minimized, especially near the desired center frequency ω_d, the energy of the residual signal should approach zero. Therefore, it is of great significance to select a suitable filter to suppress spectrum overlap. The frequency response of the filter is

$$\hat{\beta}(\omega)=\frac{1}{\mu(\omega-\omega_d^n)^2}, \tag{21}$$

where μ is the balance factor of the control bandwidth. This filter has a strong ability to suppress residuals near the target frequency, which can effectively reduce the energy leakage of the desired mode in the target frequency band, and use the penalty function J_2 to measure the energy distribution of the residual term in the frequency band.

$$J_2=\left\|\beta(t)r(t)\right\|_2^2, \tag{22}$$

where $\beta(t)$ is the time domain expression of the filter $\hat{\beta}(\omega)$. The VME extraction problem can be transformed into a constrained minimization problem, that is

$$\begin{cases}\min\limits_{u_d,\omega_d,r}\left\{\eta J_1+J_2\right\},\\ \text{s.t. } u_d(t)+r(t)=f(t),\end{cases} \tag{23}$$

where η is the parameter that balances J_1 and J_2. In order to eliminate the constraint terms, the orthogonal penalty term and Lagrange multiplier term are introduced.

$$\begin{aligned}&\mathrm{L}(u_d,\omega_d,\lambda)=\\ &\eta J_1+J_2+\left\|f(t)-(u_d(t)+r(t))\right\|_2^2+\\ &\left\langle\lambda(t),f(t)-(u_d(t)+r(t))\right\rangle,\end{aligned} \tag{24}$$

where λ is the Lagrange multiplier. The alternating direction method of the multiplication algorithm is used to iterate $u_d^{n+1}(\omega)$, ω_d^{n+1}, and λ^{n+1} to find the optimal solution. The iterative formulas are

$$\begin{cases}u_d^{n+1}(\omega)=\dfrac{f(\omega)+\eta^2(\omega-\omega_d^n)^2u_d^n(\omega)+\lambda(\omega)/2}{\left[1+(\omega-\omega_d^n)^4\eta^2\right]\left[1+2\eta(\omega-\omega_d^n)^2\right]},\\ \omega_d^{n+1}=\dfrac{\int_0^\infty\omega\left|u_d^{n+1}(\omega)\right|^2\mathrm{d}\omega}{\int_0^\infty\left|u_d^{n+1}(\omega)\right|^2\mathrm{d}\omega},\\ \lambda^{n+1}=\lambda^n+\tau\dfrac{f(\omega)-u_d^{n+1}(\omega)}{1+(\omega-\omega_d^n)^4\eta^2}.\end{cases} \tag{25}$$

When u_{d}^{n+1} satisfies the convergence conditions of Eq. (26), the effective separation of the desired mode and the residual term is finally achieved.

$$\frac{\left\| u_{\mathrm{d}}^{n+1} - u_{\mathrm{d}}^{n} \right\|_2^2}{\left\| u_{\mathrm{d}}^{n} \right\|_2^2} < \varepsilon. \tag{26}$$

In the process of variational mode extraction, the penalty factor α and the initial center frequency ω_{d} are key parameters that affect the quality of mode extraction. The penalty factor α controls the degree of energy concentration of the mode in the frequency domain, and its size directly affects the spectral distribution characteristics of the mode. If α is too large, the extracted modal spectrum will be too concentrated, resulting in the weakening of the desired main signal characteristics. On the contrary, if α is too small, the modal frequency band is too wide, and the spectrum leakage is serious, leading to the problem of modal aliasing. If the initial center frequency ω_{d} deviates too far from the main frequency of the real signal, it is easy to cause the extracted mode to be inconsistent with the actual HR signal, affecting the quality of signal decomposition. Therefore, it is important to reasonably set and select an appropriate combination of parameters to ensure the stability and accuracy of modal decomposition.

The crested porcupine optimizer (CPO) [19] has good search diversity and convergence balance due to its multi-level defense strategy, effectively avoiding falling into local optimality. Therefore, this study introduced the CPO algorithm to optimize the core parameters of VME, dynamically adjust the α value and ω_{d} within a reasonable range. CPO is a natural metaheuristic algorithm proposed by Abdel-Basset et al., which simulated the hierarchical defense behavior of crested porcupines under the threat of predation. The algorithm implements a multi-stage, balanced global and local search strategy by dividing the search area into four dynamic search areas. It has good search diversity and convergence performance and effectively avoids the risk of falling into local optimality.

This paper uses spectral energy ratio, fuzzy entropy (FE), and kurtosis as the fitness functions of the optimization algorithm.

By calculating the energy proportion of the signal in the heartbeat frequency band (0.8—2 Hz) and the respiratory frequency band (0.2—0.5 Hz) in the total frequency band, the energy proportion of the heartbeat component in the extracted signal is strengthened and the respiratory component is suppressed, which can be expressed as

$$R_{\mathrm{H}} = \frac{E_{\mathrm{heart}}}{E_{\mathrm{total}}}, \tag{27}$$

$$R_{\mathrm{R}} = \frac{E_{\mathrm{resp}}}{E_{\mathrm{total}}}, \tag{28}$$

where R_{H} is the ratio of the heartbeat frequency band, and R_{R} is the ratio of the breathing frequency band. If the energy ratio of the heartbeat frequency band is relatively high, and the energy ratio of the breathing frequency band is low, it usually means that the signal has a high purity of the heartbeat component and is suitable as a basic signal for HR estimation.

Fuzzy entropy measures the similarity between time series through an exponential membership function. Compared with traditional hard threshold entropy algorithms, it is more robust to small disturbances. Heartbeat signals are relatively regular under ideal conditions, usually showing a lower entropy value. On the contrary, if there are still more breathing and noise components in the extracted mode, the complexity of the signal increases, and the fuzzy entropy value also increases. Therefore, by designing fuzzy entropy as a component of the fitness function and minimizing its value, the heartbeat signal can be extracted with higher accuracy.

The kurtosis K can be expressed as

$$K(x) = \frac{\frac{1}{N}\sum_{i=1}^{N} x_i^4}{\left(\frac{1}{N}\sum_{i=1}^{N} x_i^2\right)^2}, \tag{29}$$

where x is the input signal and N is the length of the signal. In the extraction of heartbeat signals, the ideal heartbeat waveform usually contains an obvious pulse-type periodic structure and has a high peak feature, so the corresponding kurtosis is higher. On the contrary, respiratory components and noise often appear smooth and have relatively low kurtosis. Using kurtosis as one of the evaluation indicators can enhance the sensitivity to the sudden change characteristics of the heartbeat signal and improve the accuracy of HR estimation.

The three indicators constrain each other and are jointly optimized to ensure that the frequency structure of the extracted signal conforms to the physiological heartbeat characteristics, improves the accuracy and stability of the final HR estimation, and constructs the fitness function of the optimization problem as follows.

$$f_{\mathrm{fit}} = af_{\mathrm{E}} + bf_K + cf_{\mathrm{FE}}, \tag{30}$$

where a, b, and c are weight coefficients, the spectrum energy ratio index is $f_{\mathrm{E}} = R_{\mathrm{R}} - R_{\mathrm{H}}$, f_K is the kurtosis index, and f_{FE} is the fuzzy entropy index.

This paper uses the MUSIC algorithm to perform frequency analysis on the reconstructed heartbeat signal and extracts the main frequency component in the frequency

domain to estimate the HR. The processed expected mode $u_d(t)$ is constructed as a data matrix $\boldsymbol{Y}$ with a Hankel structure, which is convenient for extracting its time series structure and frequency characteristics.

$$\boldsymbol{Y}(:,i)=\begin{bmatrix} y(\mathrm{i}) \\ y(i+1) \\ \vdots \\ y(i+\mathrm{M}-1) \end{bmatrix},$$
$$i=1,2,\cdots,L-M+1, \tag{31}$$

where M is the window size, $M=L/2$, $\boldsymbol{Y}\in\boldsymbol{R}^{M\times(L-M+1)}$. After removing the mean of matrix $\boldsymbol{Y}$, the covariance matrix $\boldsymbol{R}$ of the signal is constructed by

$$\boldsymbol{R}=\frac{1}{L-M+1}\boldsymbol{Y}\boldsymbol{Y}^{\mathrm{H}}, \tag{32}$$

where $\boldsymbol{Y}^{\mathrm{H}}$ represents the conjugate transpose, which performs eigendecomposition on the covariance matrix, that is

$$\boldsymbol{R}=\boldsymbol{E}\boldsymbol{D}\boldsymbol{E}^{\mathrm{H}}, \tag{33}$$

where $\boldsymbol{E}=[e_1,e_2,\cdots,e_M]$ is the eigenvector matrix corresponding to $\boldsymbol{R}$, $\boldsymbol{D}$ is the eigenvalue diagonal matrix. Sort the eigenvalues from large to small, the first d are the signal subspace, and the rest are the noise subspace. The noise subspace is constructed as

$$\boldsymbol{E}_{\mathrm{n}}=[e_{d+1},e_{d+2},\cdots,e_M]. \tag{34}$$

For each frequency point $f_k\in[0,f_s/2]$ (f_s is the sampling frequency 20 Hz), construct the corresponding steering vector $a(f_k)$ to determine the orthogonality between the signal and noise subspaces.

$$a(f_k)=[\mathrm{e}^{-\mathrm{j}2\pi\mathrm{f_k}/f_s}]_{\mathrm{n}=0}^{\mathrm{M}-1}. \tag{35}$$

Therefore, the MUSIC power spectrum can accurately locate the frequency components of the signal.

$$P_{\mathrm{MUSIC}}=\frac{1}{a(f_k)^H\boldsymbol{E}_n\boldsymbol{E}_n{}^Ha(f_k)}. \tag{36}$$

By performing a peak search on the MUSIC power spectrum, the main peak position can be effectively identified, and the frequency corresponding to the main peak is the dominant frequency component of the heartbeat. Compared with the traditional FFT method, the MUSIC algorithm has a higher frequency resolution. As shown in Fig.10, when using FFT for spectrum analysis, there are two peaks with similar frequencies and amplitudes, making it difficult to distinguish the main peak of the heartbeat; after using MUSIC to perform spectrum analysis on the same signal, there is an obvious and sharp main peak at 1.24 Hz, which can accurately identify the main frequency of the heartbeat in the presence of multiple interferences, thereby improving the accuracy of HR estimation.

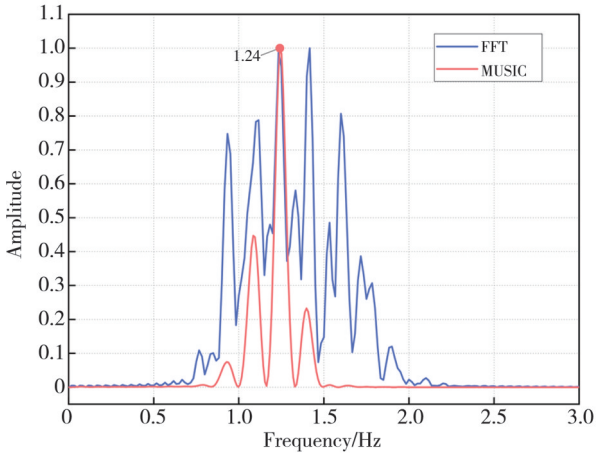

Fig. 10 Spectrograms analyzed by different algorithms

3 Results and discussion

3.1 Experimental equipment and environment

This study used the AWR 1843Boost millimeter-wave radar sensor from TI (Texas instruments) and the DCA1000EVM to collect raw data from the millimeter-wave radar, to determine the presence of human body and to perform non-contact detection of vital signs, and to use the HR data collected by a medical monitor (Cofoe Medical Technology Co., LTD, KF12) as a reference value, as shown in Fig.11. This paper uses a single-transmit and single-receive antenna configuration. The specific radar parameter configuration is shown in Table 1.

Table 1 Radar parameters

Parameter	Value
Start frequency/GHz	77
Frequency slope/(MHz·μs^{-1})	58.998
Bandwidth/MHz	3 020.698
ADC sampling rate/kilo samples per second	5 000
ADC samples	256
Range resolution/m	0.05
Frame frequency/ms	50
Idle time/μs	100

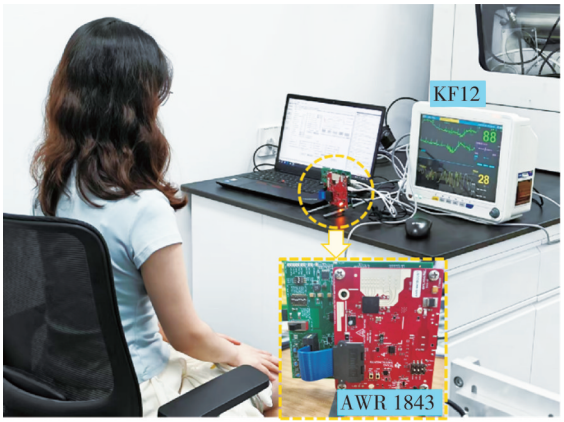

Fig. 11 Experimental environment

3.2 Analysis of results of human presence

In order to verify the effectiveness of the algorithm in the problem of judging the presence of the human body, this study designs two types of experimental scenarios: a human body persistent scenario and a state change scenario.

1) Human body persistent scenario. In order to evaluate the algorithm's judgment robustness under the condition of a constant human body, two constant experimental scenarios were constructed, one in which there was always a human body in the detection area, and the other in which there was no one in the detection area. In each case, 10 groups of data samples with a duration of 60 s were collected. Since a 10-second sliding window was used for data processing, each group of data samples can obtain effective detection results for 50 s. 2) State change scenario. In order to evaluate the algorithm's judgment accuracy under the condition of personnel state changes, data with a duration of 60 s was collected. After some time, the human target left or entered the area to be tested, and the state switching process was constructed. Multiple groups of data are collected separately, and the situation where the human target was located in different positions in the detection area was considered to fully verify the accuracy of the personnel presence judgment algorithm under different position distributions.

As shown in Fig. 12, the upper figure is a distance-time diagram within the detection range, which clearly reflects the dynamic changes of the human body. There is no target in the detection area in the first 22 s. At 22 s, the human body begins to enter the detection range. At 22 s, the human body state remains stable at 0.7 m, and the target position is relatively stable from this moment to 50 s. The figure below is a diagram of the person presence judgment result based on the output of the proposed algorithm. "1" indicates that a person is detected, and "0" indicates that a person is not present. The result shows that before 22 s, the stable output is "0", and the detection result is that no one is present. After 22 s, the stable output is "1", and the detection result is that someone is present.

To evaluate the performance of the proposed algorithm, the experiments adopt miss rate R_M and false alarm rate R_A as evaluation metrics.

$$R_M = \frac{N_1}{N} \times 100\%, \tag{37}$$

$$R_A = \frac{N_2}{N} \times 100\%, \tag{38}$$

where N is the total number of samples, N_1 is the number of missed results, and N_2 is the number of false alarm results.

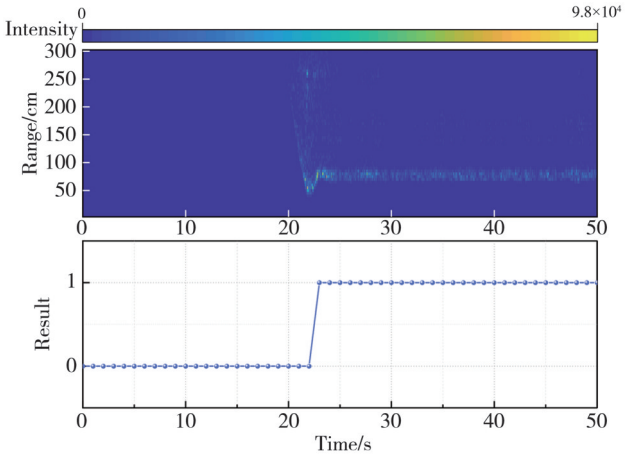

Fig. 12 Range-dimension data from no human to human presence and result decision diagram

In Table 2, the miss rate under the condition of always having people and the false alarm rate under the condition of always having no people are calculated, respectively, and the average values are calculated to characterize the algorithm's judgment accuracy in the scenarios of continuous presence and continuous absence. From the results, the average miss rate of the algorithm in the scene where there are always people is 2.2%, and the false alarm rate in the scene where there are no people is 3.2%, which shows that the proposed algorithm can output results stably under the condition that the human target state is constant. As shown in Table 3, to evaluate the detection capability of target state changes at different positions within the detection range, the experiment set up personnel state transition scenarios at 0.5 m, 1 m and 1.5 m away from the radar, covering two scenario changes: "from unmanned to manned" and "manned to unmanned". The results show that the average judgment accuracy of the transition from manned to unmanned state is 93.1%, and the average judgment accuracy of the transition from unmanned to manned state is 90.7%, it shows better detection performance under closer distance conditions.

Table 2 Results in persistent human/non-human target scenarios

Number of experiments	With human, R_M/%	Without human, R_A/%
1	0	6
2	0	0
3	0	6
5	0	0
6	0	0
7	6	0
8	0	0
9	0	6
10	8	8
Average value	2.2	3.2

Table 3 Accuracy of target state transitions at different distances

Scenario	Range/m	Accuracy/%
Human departure	0.5	95.3
	1	92.7
	1.5	91.3
Average value		93.1
Human arrival	0.5	94.7
	1	89.3
	1.5	88
Average		90.7

3.3 Analysis of HR estimation experimental results

The HR estimation experiments were all conducted in the laboratory, with the subjects sitting quietly 0.5 m in front of the radar. To evaluate the performance of the HR algorithm in this paper, the root mean square error (RMSE) and mean absolute error (MAE) were used to measure the error between the estimated value and the reference value.

$$RMSE=\sqrt{\frac{1}{N}\sum_{i=1}^{n}\left(Y(i)-y(i)\right)^{2}}, \tag{39}$$

$$MAE=\frac{1}{N}\sum_{i=1}^{n}\left|Y(i)-y(i)\right|, \tag{40}$$

where Y represents the reference value of HR, y represents the estimated HR value of the radar, and N is the number of samples.

In order to verify the optimization performance of the CPO algorithm, this study introduced two classic group intelligence optimization algorithms, particle swarm algorithm (PSO) and whale optimization algorithm (WOA), for comparison. Under the constraint of the same fitness function, the fitness values obtained by each algorithm were compared and analyzed. As shown in Fig.13, the PSO algorithm converges slightly faster than the CPO algorithm at the beginning, but falls into the local optimal solution many times after a certain number of iterations; the WOA algorithm converges slowly in the early stage, and similarly, falls into the local optimal solution after a certain number of iterations; in comparison, the CPO algorithm not only has a faster overall convergence speed, but can also effectively avoid falling into the local optimal solution, showing stronger optimization ability and convergence stability.

We also compared the proposed improved algorithm with the traditional fixed-parameter VME[20] algorithm. Fig. 14 shows the reference HR value measured by the monitor, the HR value estimated by the improved VME, and the HR value estimated by the fixed parameter VME. The HR curve estimated by the improved VME is closer to the reference HR curve, while the HR curve estimated by the fixed parameter VME has a significant offset, and obvious abnormal values appear at 2 s, 10 s, and 33 s. This may be due to the fine-tuning of the human target's posture, the offset of the main HR frequency, and the lack of adaptive ability of the fixed parameter VME, resulting in feature extraction failure.

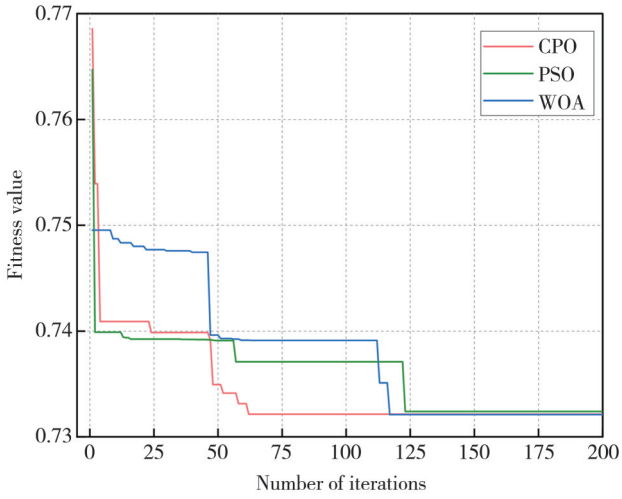

Fig. 13 Fitness curve of optimization algorithm

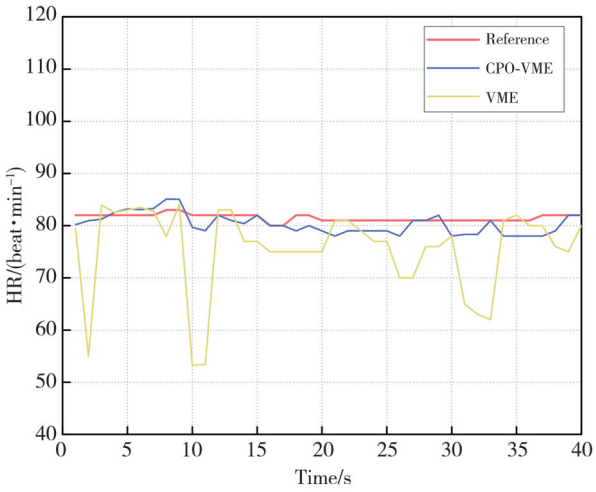

Fig. 14 Comparison of estimated values from different algorithms with reference values

To verify the algorithm's adaptability to individual differences, multiple test subjects were tested, and their heart rate signals were collected and processed using millimeter wave radar. Fig. 15 shows a bar chart comparing the RMSE and MAE results of 20 test subjects under the two methods. It can be seen that the algorithm proposed in this paper has a smaller estimation error between different subjects, and the average reduction values of RMSE and MAE are 3.39 beat per minute and 3.26 beat per minute, respectively. This result verifies its good adaptability to individual differences.

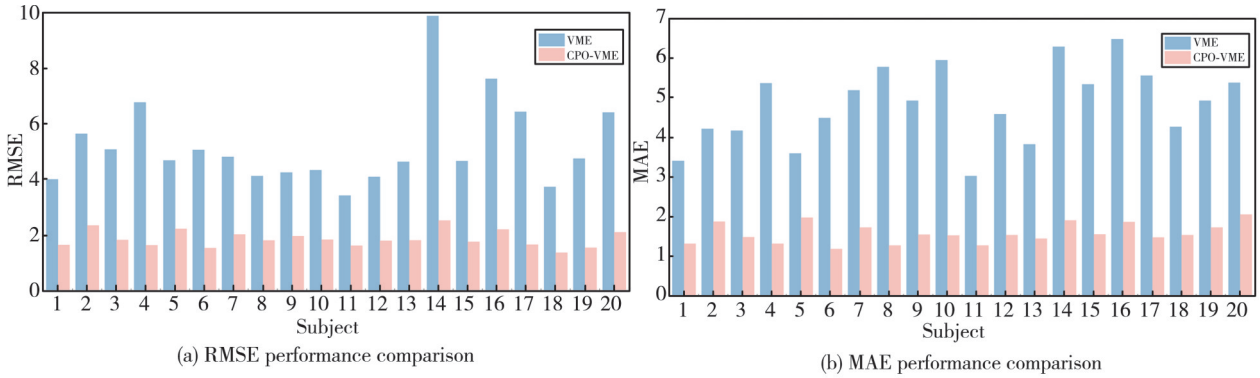

(a) RMSE performance comparison (b) MAE performance comparison

Fig. 15 Performance comparison of heart rate estimation algorithms across 20 subjects

As can be seen from Fig.16, in the long-term detection of 200 s, the HR curve estimated by the algorithm in this paper shows a relatively consistent trend with the actual HR, without obvious abnormal HR jumps, and has good stability in the long-term detection scenario.

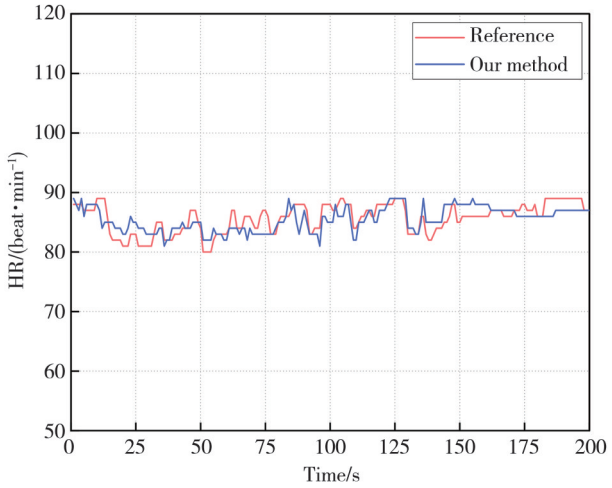

Fig. 16 Comparison between algorithm estimated values and reference values within 200 s

4 Conclusions

We proposed a human body presence judgment algorithm and an improved VME algorithm. Given the difficulty in distinguishing human body from background noise in a quiet state, an adaptive dual-threshold human body presence judgment algorithm based on low-frequency energy ratio was designed. The algorithm can make adaptive adjustments according to the low-frequency energy in the actual collected signal, automatically optimize the judgment criteria under different background noises, and significantly improve the robustness of presence judgment. The results show that the proposed algorithm has high judgment stability in the case of continuous presence of people and in an empty environment, and also has good judgment accuracy in the human target state transition scenario. A millimeter wave radar heart rate detection algorithm based on an improved VME algorithm combined with MUSIC spectrum analysis was also proposed. CPO was used to optimize the parameters of VME, which solved the problem of parameter setting dependence on experience and poor adaptability. The use of MUSIC high-resolution algorithm made spectrum estimation more stable and improved the accuracy of heart rate estimation.

In this study, most existing work has focused on relatively simple scenarios, without fully considering the impact of complex environments—such as multi-source interference and dynamic backgrounds—on algorithm performance. However, these factors are critical in practical applications. For example, commonly used appliances in home environments may generate low-frequency signals similar to human micro-movements, potentially interfering with detection accuracy. Therefore, future research could incorporate neural network models to learn nonlinear features across diverse scenarios, enabling more effective differentiation between human micro-movements and complex background noise, and further enhancing the robustness of human presence detection and heart rate estimation in complex environments.

Acknowledgement

This work was supported by National Natural Science Foundation of China (Nos. 62320106002 and U22A2014), National Key Research and Development Program of China (No. 2021YFA1401103), 2022 Wuxi Taihu Talent Program: Innovative Leading Talent Team (No.1096010241230120).

Declaration of conflicting interests

The authors have no conflicts of interest related to this publication.

References

[1] MASHHADIGHOLAMALI M, FARD A S, ZOLFAGHARI S, et al. FMCW radar-based human activity recognition: a machine learning approach for elderly care// 2025 IEEE Wireless Communications and Networking

Conference, March 24-27, 2025, Milan, Italy. New York: IEEE, 2025: 1-6.
[2] CHEN C R, DING S C, WANG J. Digital health for aging populations. Nature Medicine, 2023, 29(7): 1623-1630.
[3] LI A N, BODANESE E, POSLAD S, et al. A contactless health monitoring system for vital signs monitoring, human activity recognition, and tracking. IEEE Internet of Things Journal, 2024, 11(18): 29275-29286.
[4] CAO Y J, WANG F C, LU X X, et al. Contactless body movement recognition during sleep *via* WiFi signals. IEEE Internet of Things Journal, 2020, 7(3): 2028-2037.
[5] ZHANG J, YU J, MA Y, et al. RF-RES: Respiration monitoring with COTS RFID tags by dopplershift. IEEE Sensors Journal, 2021, 21(21): 24844–24854.
[6] ALIZADEH M, SHAKER G, DE ALMEIDA J C M, et al. Remote monitoring of human vital signs using mm-wave FMCW radar. IEEE Access, 2019, 7: 54958-54968.
[7] TU J X, HWANG T, LIN J. Respiration rate measurement under 1-D body motion using single continuous-wave Doppler radar vital sign detection system. IEEE Transactions on Microwave Theory and Techniques, 2016, 64(6): 1937-1946.
[8] REN L Y, WANG H F, NAISHADHAM K, et al. Phase-based methods for heart rate detection using UWB impulse Doppler radar. IEEE Transactions on Microwave Theory and Techniques, 2016, 64(10): 3319-3331.
[9] XUE W, WANG R, LIU L, et al. Accurate multi-target vital signs detection method for FMCW radar. Measurement: Journal of the International Measurement Confederation, 2023, 223(October): 113715.
[10] LI Q, LIU J, GRAVINA R, et al. A UWB-Radar-Based Adaptive Method for In-Home Monitoring of Elderly. IEEE Sensors Journal, 2024, 11(4): 6241-6252.
[11] YAN K, WU S Y, YE S B, et al. A novel wireless-netted UWB life-detection radar system for quasi-static person sensing. Applied Sciences, 2021, 11(1): 424.
[12] XU D, MEMBER S, YU W, et al. Vital signs detection in the presence of nonperiodic body movements. IEEE Transactions on Instrumentation and Measurement, 2024, 73: 1-16.
[13] DEIANA D, SUIJKER E M, BOLT R J, et al. Real time indoor presence detection with a novel radar on a chip//2014 International Radar Conference, October 13-17, 2014, Lille, France. New York: IEEE, 2015: 1-4.
[14] REGEV N, WULICH D. Radar-based, simultaneous human presence detection and breathing rate estimation. Sensors, 2021, 21(10): 3529.
[15] LI D, HUANG Y, LI H, et al. A novel approach to accurate respiratory rate and heart rate estimation via FMCW radar. IEEE Sensors Journal, 2025, 25(8): 13937-13945.
[16] QU L L, LIU C Y, YANG T H, et al. Vital sign detection of FMCW radar based on improved adaptive parameter variational mode decomposition. IEEE Sensors Journal, 2023, 23(20): 25048-25060.
[17] DUAN X, LI K P, LIU X, et al. A noncontact sleep monitoring method based on millimeter-wave radar. IEEE Transactions on Instrumentation and Measurement, 2025, 74: 4006410.
[18] NAZARI M, SAKHAEI S M. Variational mode extraction: a new efficient method to derive respiratory signals from ECG. IEEE Journal of Biomedical and Health Informatics, 2018, 22(4): 1059-1067.
[19] ABDEL-BASSET M, MOHAMED R, ABOUHAWWASH M. Crested porcupine optimizer: a new nature-inspired metaheuristic. Knowledge-Based Systems, 2024, 284: 111257.
[20] ZHOU M, LIU Y X, WU S E, et al. A novel scheme of high-precision heart rate detection with a mm-wave FMCW radar. IEEE Access, 2023, 11: 85118-85136.

基于毫米波雷达的人员存在判断与心率估计算法

朱新星[1], 高翊轩[1], 李明潮[1], 武恩康[1], 顾晓峰[1], 梁峻阁[1,2*], 喻　甜[1*], 王　琮[3]

1. 江南大学 集成电路学院, 江苏 无锡 214122;
2. 光云大学 RFIC中心, 韩国 首尔 01897;
3. 哈尔滨工业大学 电子与信息工程学院, 黑龙江 哈尔滨 150001

摘　要： 针对智慧养老场景中人员是否存在的问题，本文提出了一种基于自适应双阈值的人员存在判决方法，以减少对空环境进行无效的生命体征检测。该方法以低频能量比作为核心判断依据，结合自适应阈值，实现对人体目标存在的准确判断，有效降低了因背景干扰引起的误检。此外，针对变分模态提取（VME）需要依赖经验值手动调参的缺陷，引入冠豪猪优化算法（CPO）对VME参数自适应优化，并使用优化后的VME重构心跳信号，提高信号纯净度。然后，使用多重信号分类（MUSIC）算法做频谱分析，提高心率估计准确度。结果表明，在人员实验判决中，有人情况下的漏报率为2.2%，无人情况下的判断误报率仅为3.2%；所提出的心率估计方法相比于传统VME的均方根误差和平均绝对误差分别降低了4.4次/分和3.05次/分，验证了其优异性。

关键词： 人员存在判决；FMCW雷达；自适应双阈值；改进VME；多重信号分类

引用格式： ZHU Xinxing, GAO Yixuan, LI Mingchao, et al. Human presence detection and heart rate estimation algorithm based on millimeter-wave radar. Journal of Measurement Science and Instrumentation, 2025, 16(4): 473-485. DOI: 10.62756/jmsi.1674-8042.2025046